Impact of Hygrothermal Aging on Structure/Function Relationship of Perfluorosulfonic-Acid Membrane

Shouwen Shi,[1,2] Thomas J. Dursch,[1] Colin Blake,[1] Rangachary Mukundan,[3] Rodney L. Borup,[3] Adam Z. Weber,[1] Ahmet Kusoglu[1]

[1]Energy Storage and Distributed Resources Division, Lawrence Berkeley National Laboratory, 1 Cyclotron Road, Berkeley, California 94720
[2]School of Chemical Engineering and Technology, Tianjin University, Tianjin 300072, China
[3]Los Alamos National Laboratory, MS D429, MST-11, Los Alamos, New Mexico 87545
Correspondence to: A. Kusoglu (E-mail: akusoglu@lbl.gov)

Received 30 June 2015; accepted 6 October 2015; published online 20 October 2015
DOI: 10.1002/polb.23946

ABSTRACT: Perfluorosulfonic-acid (PFSA) membranes are widely used as the solid electrolyte in electrochemical devices where their main functionalities are ion (proton) conduction and gas separation in a thermomechanically stable matrix. Due to prolonged operational requirements in these devices, PFSA membranes' properties change with time due to hygrothermal aging. This paper studies the evolution of PFSA structure/property relationship changes during hygrothermal aging, including chemical changes leading to changes in ion-exchange capacity (IEC), nanostructure, water-uptake behavior, conductivity, and mechanical properties. Our findings demonstrate that with hygrothermal aging, the storage modulus increases, while IEC and water content decrease, consistent with the changes in nanostructure, that is, water- and crystalline-domain spacings inferred from small- and wide-angle X-ray scattering (SAXS/WAXS) experiments. In addition, the impact of aging is found to depend on the membrane's thermal prehistory and post-treatments, although universal correlations exist between nanostructural changes and water uptake. The findings have impact on understanding lifetime, durability, and use of these and related polymers in various technologies. © 2015 Wiley Periodicals, Inc. J. Polym. Sci., Part B: Polym. Phys. **2016**, *54*, 570–581

KEYWORDS: hygrothermal aging; ion-exchange capacity; PFSA ionomers; SAXS/WAXS; structure/property

INTRODUCTION Perfluorosulfonic-acid (PFSA) membranes are the most widely used ionomer for polymer-electrolyte fuel-cell (PEFC) applications as well as for other electrochemical energy storage and conversion devices such as redox flow batteries. Nafion® membrane, a commercial PFSA ionomer, has been long considered the benchmark material for not only understanding the role of ion-conductive polymers in PEFCs, but also for developing alternative materials. Nafion® membrane's high proton conductivity and mechanical stability are critical factors for achieving cell performance and durability targets, respectively. In PEFCs, the chemical and mechanical stressors are coupled, are strongly affected by temperature and humidity, and their impact dependent on the membrane's hygrothermal history, therefore making it difficult to characterize the role of individual stressors on overall properties.[1–7] It is of particular interest to uncouple the effects of hygrothermal aging, that is prolonged exposure to hot and humid environments, from those of chemical degradation to understand better the mechanistic origins controlling the membrane's response and operational lifetime.

PEFCs are frequently subjected to hydration/dehydration and electrochemical-potential cycles at high temperatures during operation,[2,4,6–8] which can alter the properties of the polymer electrolyte.[3,8–12] During such aging, a decay in conductivity has been observed,[9,10,13] as well as a decrease in water uptake and increase in tensile modulus,[3,8,10,12] which is thought to be due to either contamination or the formation of crosslinked sulfonic anhydrides via condensation of side-chain sulfonic-acid (SO_3^-) groups (Fig. 1).[3,9–11] Therefore, it is expected that an aged membrane, which contains these additional crosslinks, to exhibit an increase in mechanical stability and modulus but a decrease in transport-related properties. Interestingly, the effect of aging was shown to be more pronounced for membranes aged in higher relative humidity (RH) than dry (i.e., 0% RH) conditions.[3,10] Acceleration of anhydride formation or related chemical changes at

Additional Supporting Information may be found in the online version of this article.

higher humidities could be attributed to the fact that water could act as a plasticizer promoting side-chain mobility and changing the distance between the pendant groups.[10] However, if the membrane's water content is too high, as in the case of immersion in liquid water, the effect of aging is reduced, where it has been suggested that the mechanism of anhydride hydrolysis might be dominant or the distance between the side-chains could become too large to allow condensation reactions.[10]

The effect of hygrothermal aging is reversible in that it can be erased in the presence of strong acid, but not just in DI water.[8,14] Such acid-treatment of aged membranes was reported to recover the aging-induced losses in water uptake and mechanical properties, as well as PEFC performance.[8] Thus, it seems that water content and thermal history all play significant roles in controlling the impact of aging on membrane properties. It is worth noting that mechanisms such as SO_3^- condensation could be active in other chemical degradation modes due to the operating conditions. It was observed that a PFSA membrane's modulus increases more with lower humidity operation under OCV aging,[4,15,16] which might be again due in some part to possible S—O—S cross-linking, along with other chemical degradation reactions. Likewise, hygrothermal aging could impact similar membranes in different technological applications such as membrane humidifiers.

It has been well documented that the morphology and transport properties of even fresh membranes are strongly influenced by their thermal history.[3,8,17–19] The water uptake,[20–23] permeability,[22] diffusivity,[21] conductivity,[21–24] and mechanical properties,[19,21] along with phase-separated nanostructure,[19,21,25,26] all change depending on the membrane's thermal history, which can be altered through heat-treatment processes such as (pre)boiling in liquid water or dry, high-temperature annealing. For example, small-angle X-ray scattering (SAXS) data showed that preboiling a PFSA membrane increases its water-domain spacing as compared to an as-received one, consistent with the observed increase in water uptake.[27,28] Thus, such thermal-treatment effects are likely to be more influential in the presence of aging, during which the structure/property relationship(s) change over time. Unfortunately, most of the aging data in the literature were obtained using as-received membranes, thus there is a strong need to understand how thermal history impacts aging observations. While it is better to pretreat the as-received membranes to establish a baseline and reset a membrane's thermal history,[21,26,27,29] this does not necessarily represent the membrane state in a PEFC assembly, wherein it is hot-pressed during the membrane–electrode assembly (MEA) formation process. Thus, there is an additional need to explore alternative treatment methods that mimic the thermal-treatments a membrane is exposed to during MEA formation. Therefore, determining the influence of membrane pretreatment on subsequent hygrothermal aging is an important step toward developing a better understanding for an ionomer membrane's degradation behavior *in operando*.

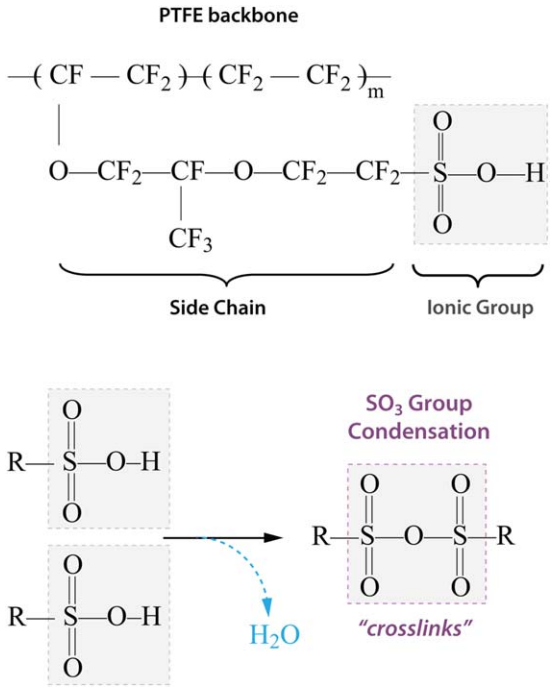

FIGURE 1 Chemical structure of Nafion PFSA and process of anhydride formation through sulfonic-acid group condensation. [Color figure can be viewed in the online issue, which is available at wileyonlinelibrary.com.]

This paper reports a systematic investigation of the effects of aging and pretreatment conditions on a membrane's structure/function relationship. In particular, water uptake, conductivity, mechanical behavior, and nanostructure are investigated to determine the true influence of aging, including the impact of pre-/post-treatments. Finally, the discussion links the various data to elucidate the underlying phenomena and governing relationships for this class of polymer.

EXPERIMENTAL

Membrane and Aging

Nafion® 212 membranes with 2 mil (~51 μm) nominal thickness and 1100 g/mol (SO_3^-) equivalent weight (EW) or 0.909 mmol/g ion-exchange capacity (IEC) were received in protonated (H^+) form from Ion Power (New Castle, DE). In addition to these as-received (AsR) samples, pretreated (PT) samples were prepared using the standard pretreatment procedure (boiled in 0.5M H_2SO_4 and then in DI H_2O for 1 h each) as described previously.[30] Lastly, to set a baseline for cell-assembly conditions, as-processed (AsP) membranes were prepared by hot pressing the pretreated membranes for 5 min at 700 psi and 130 °C such that the membrane undergoes the same thermomechanical deformation process as that during membrane–electrode assembly (MEA) fabrication. Membranes that were not aged are referred to as "fresh" samples.

TABLE 1 Sample Matrix for Nafion 212 Membranes, Based on the Pretreatment Conditions and Hygrothermal Aging Protocols Used in this Study

Pretreatment		Aging	EW (g/mol)	IEC[a] (meq/g)
As-received	AsR	Fresh	1062 ± 49	0.94
		Aged	1250 ± 33	0.80
Pretreated (protonation + water boiling)	PT	Fresh	1237 ± 70	0.81
		Aged	1334 ± 126	0.75
As-processed (pretreated + hot-pressed)	AsP	Fresh	1102 ± 113	0.91
		Aged	1305 ± 67	0.76

[a] Average.

The hygrothermal aging of membranes was conducted in environmental chambers constructed from solid cylinders of PTFE. Membranes were placed in a nylon mesh and suspended in an environmental chamber. The aging was conducted at 80 °C, with a continuous air flowrate of 0.5 L/min and an average residence time of 6 min. The inlet gas was humidified by saturating it by sparging through DI water set to the temperature corresponding to the desired dew point of the inlet gases. The membrane samples were aged at 100% RH for 150 h. For PT membranes, selected aged samples were boiled in DI water or in 0.5M H_2SO_4 to investigate the effect of post-treatments and recovery. The treatment and aging conditions are summarized in Table 1.

Titration

Membrane EWs were determined by acid-base titration following Chen and Leddy.[31] Membranes were either used as-is or following boiling in concentrated acid. The latter were prepared by gently boiling as-is membranes (~15 mg) in 1M hydrochloric acid and then in DI water (to remove excess acid) for 1 h each. In all cases, membranes were placed into excess 1M NaCl solutions (with a 5:1 solution volume: membrane mass ratio) for 24 h to convert samples from H^+ to Na^+ form. Samples were then removed from solution and dried in 0% RH at 25 °C for 48 h to determine the membrane dry weight, M_0. Resulting NaCl solutions were titrated against 0.1N sodium hydroxide (NaOH, Sigma Aldrich, Cat. No. 38212-1L) in 10 μL increments using a micropipette. The aqueous solution pH was measured using a hand-held Oakton pH meter (Oakton Instruments, Vernon Hills, Il, Cat. No. WD-35613-00). Assuming complete sodium exchange, membrane equivalent weight was calculated from the moles of 0.1N NaOH consumed at the equivalence point by: EW = M_0/mol (NaOH).[32,33]

FTIR

FTIR spectra were collected at room temperature on a Nicolet 8700 FT-IR spectrometer from Thermo Fisher in Attenuated Total Reflectance (ATR) mode using a Diamond window and ZnSe window. A total of 64 interferograms were signal averaged to obtain each spectra and with spectra collected at a resolution of 2.0 and gain of 8.0 and optical velocity of 0.63 within the range of 4000–500 cm^{-1} with a spectral resolution of 4 cm^{-1}. Spectral analysis included integration of the 1440 cm^{-1} anhydride peak from 1390 to 1473 cm^{-1}.

Water Uptake

Membrane water uptake was measured as a function of RH using a dynamic-vapor-sorption (DVS) analyzer (Surface Measurement Systems, UK).[27,29] All samples were first dried in 0% RH at 25 °C for 2 h to set and determine the dry weight of the sample, M_0. The sample was then humidified in a controlled environment with increasing RH intervals of 10–90%, and then to 95 and 98%. Samples were then dehumidified back to 0% following the same RH values and time intervals. The samples were equilibrated at each RH step for at least 2 h or until the change in the weight, $\Delta M/M_0$, was less than 0.005%/min. Liquid-water uptake of the membrane was determined as a function of temperature by heating the samples in liquid water from 25 to 40, 60, 80, and 90 °C. The samples were equilibrated in liquid water at least 20 min, and their weight and thickness were recorded immediately after they were taken out of the water and the surface water wiped off. The process was repeated using the same sample for all temperatures. The weight of water absorbed by the sample, ΔM_w, was determined from the measured stable weight at target humidity, M, and the initial weight, M_0. Water content, λ, that is, the number of water molecules per sulfonic-acid group of ionomer,[34] is calculated by

$$\lambda = \frac{\text{mol}(H_2O)}{\text{mol}(SO_3)} = \frac{\Delta M_w/18}{M_0/\text{EW}} \quad (1)$$

where EW [g/mol] is the actual equivalent weight of the sample determined by titration and 18 g/mol is the molar mass of water.

Mechanical Properties

Mechanical properties of fresh and aged membranes were studied using a dynamic mechanical analyzer (DMA-Tritec 2000). Samples were analyzed in tension mode with a frequency of 1 Hz and a heating rate of 5 °C/min. At least two measurements were carried out for the samples. Storage modulus and tan(δ) were measured as a function of temperature (25–200 °C). In general, *storage modulus*, denoted as E', is a measure of the elastic character of the material and is related to its stiffness; whereas *loss modulus*, denoted as E'', is a measure of the viscous nature of the material and

reflects the damping capacity of the material. Tan(δ), the ratio of the loss modulus to the storage modulus, is indicative of the ratio of energy dissipated to energy stored per cycle of deformation.[35]

Conductivity

The through-plane (thickness direction) proton conductivity was measured using a Membrane Test System (MTS) (MTS740, Scribner Associates). The MTS uses AC impedance measurements under controlled humidity and temperature using an SI 1260 impedance/gain-phase analyzer (Schlumberger Technologies) and ZPlot software (Scribner Associates). Detailed description of this setup is given elsewhere.[36] Samples were prepared by cutting the membrane into 10 $\times$ 30 mm pieces which were compressed between gas-diffusion electrodes (GDE) (IRD Fuel Cell Technology) that are attached to the platinum source electrodes with conductive carbon paint. The sample was then compressed between electrodes with a load of approximately 2.15 ± 0.017 MPa (310 ± 2.5 psi) measured by a calibrated force spring and dial displacement indicator. The test procedure below was adapted from that described and used by Cooper.[36] The samples were first preconditioned at 70% RH under nitrogen atmosphere at 30 °C for 2 h. The samples were then dehumidified with 10% intervals down to 20%, followed by humidified up to 90% then 95 and 98% RH—similar to the protocol used for the water-uptake measurements. Samples were held for 30 min at each step before measuring membrane resistance. The impedance was measured using voltage controlled frequency sweep spectroscopy (10 mV_{AC} at 0 V_{DC}, 1 MHz to 1 Hz, 10 steps/decade). The conductivity is obtained from $\kappa = L/RA$, where L is the thickness of the membrane, which was measured at ambient conditions, R is the resistance derived from the high-frequency intercept of the impedance with the real axis, and A is the overlapping area of the electrodes (0.5 cm^2).

In-plane conductivity was measured using a four-electrode BT-110 conductivity clamp (Scribner Associates) in liquid water. Membranes were cut into strips and placed in the clamp. AC impedance data were collected using a BioLogic VSP potentiostat over a frequency range of 20 mHz to 1 MHz at a bias of 100 mV. Membranes were submersed in water for at least 1 h before each measurement to allow membrane equilibration. Membrane conductivity was calculated as $\kappa = L_{IP}/R_{IP}A_{IP}$, where L_{IP} is the distance between voltage measurements leads (0.425 cm), R_{IP} is the resistance of the sample, and A_{IP} is the cross section area of the sample.

Nanomorphology

Small/wide-angle X-ray scattering (SAXS/WAXS) experiments were carried out in beamline 7.3.3 of the Advanced Light Source (ALS) at Lawrence Berkeley National Laboratory (LBNL) to determine the phase-separated nanomorphology of the membrane. The X-ray wavelength used was $\lambda = 0.124$ nm, with a monochromator energy resolution of E/dE of 100, and the presented patterns were collected using a 2D Dectris Pilatus 2M CCD detector (172 $\times$ 172 μm pixel size). The scattering wave vector, $q = 4\pi \sin(\theta/2)/\lambda$, where θ is the scattering angle, was in the range of 0.01–0.03 $Å^{-1}$ for SAXS and 0.1–3 $Å^{-1}$ for WAXS. SAXS images for vapor- and liquid-equilibrated samples were obtained *in situ* using custom-designed temperature-controlled solution cells with X-ray transparent Kapton™ windows. For liquid-water heating experiments, samples were placed in the solution cells with liquid water and equilibrated for at least 1 h at 25 °C, then SAXS images were collected at various temperatures during heating from 25 to 90 °C. WAXS images were obtained under ambient conditions at room temperature using the same sample holders. The two-dimensional scattering patterns were azimuthally integrated to generate 1-D intensity profiles, $I(q)$, which were corrected for background scattering. From the SAXS data, hydrophilic-domain spacing and intercrystalline spacing are calculated by using a Gaussian fit to the peaks. The relative degree of the crystallinity, χ_{cryst}, is calculated from the relative area of the crystalline and amorphous peaks, which are determined after the deconvolution of the WAXS peak, using[37]

$$\chi_{cryst} = \frac{A_{crystalline}}{A_{crystalline} + A_{amorphous}}, \; A_r = \int_A q^2 I_r(q) dq \qquad (2)$$

where A_r represents the integration of the peak intensities under the region r (i.e., crystalline or amorphous).

RESULTS

Formation of Functional Species and Changes in Equivalent Weight

FTIR data for fresh and aged Nafion membranes for various pretreatments are summarized in Figure 2. The data demonstrate that hygrothermal aging leads to the formation of a functional group as witnessed by a new FTIR adsorbance at 1440 cm^{-1}, which has been assigned as an anhydride species as shown in Figure 1.[8,9] These results are consistent with those of Clapham et al.,[9] who also attributed this peak to S═O anhydride band formation after aging of various PFSA chemistries. After aging, a membrane's EW increases, concomitant with the formation of the functional species observed by the FTIR spectra and subsequent decrease in" free" sulfonic acid groups (see Table 1 and Fig. 3). From the values, pretreatment appears to have little quantitative impact on the measured EWs, which are close to the nominal value (1100 g/mol), especially when the EW is measured after the samples are boiled. Hygrothermal aging increases the EW for the AsR membranes, which is consistent with previous studies reporting an increased EW for aged AsR Nafion membrane,[3,9,10] as well as for the PT and AsP membranes, which has not been previously reported. From the FTIR and EW data, it can be inferred that PT membranes are less susceptible to anhydride formation upon aging, compared to AsR and AsP membranes. However, the AsP membrane, which was pretreated and then hot-pressed, exhibits the most increase upon aging, meaning that the hot-pressing processing makes the membrane more vulnerable to aging-

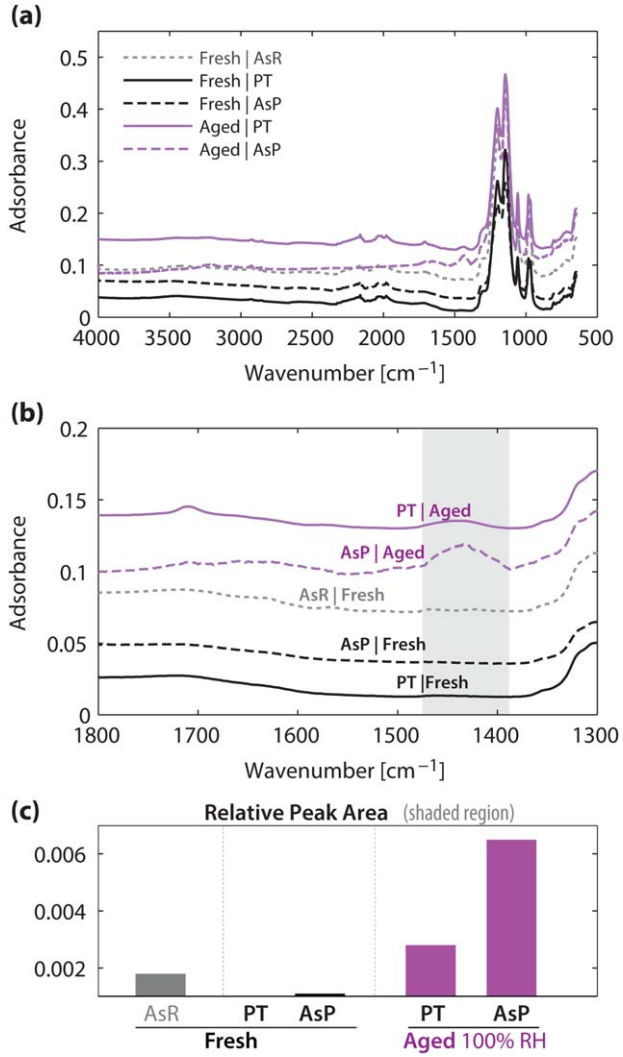

FIGURE 2 FTIR profiles for selected fresh and aged Nafion 212 membranes (a, b). Integrated peak values for the functional species formed at 1440 cm^{-1} are plotted in c. [Color figure can be viewed in the online issue, which is available at wileyonlinelibrary.com.]

induced changes in morphology either through the thermal treatment or perhaps contamination.

However, after boiling in acid and water, the increase in EWs of the aged membranes disappeared, regardless of the pretreatment. Thus, thermal history of the membrane is critical in that pretreatment may not only influence EW for the fresh membrane, but, more importantly, affect how the membrane's IEC changes during aging.

When compared to the baseline value of 1100 g/mol, the fact that aging increases the membrane's EW (i.e., less accessible SO_3^- groups), which then decreases (i.e., more accessible SO_3^- groups) after the aged membrane is boiled implies/reveals somewhat recoverable changes in the membrane's sulfonic-acid-group capacity during aging, although it should be noted that titration has some inherent error for EW measurements as previously discussed.[38]

Mechanical Properties

The dynamic mechanical response of the membranes as a function of temperature was investigated to study the impact of aging (Fig. 4). Nafion membranes possess a broad thermo-mechanical transition in their dynamic mechanical analysis curve,[17] with the peak of the transition referred to as the alpha transition temperature, T_α, which is attributed to the long-range mobility of the main and side chains through the significant weakening of the electrostatic interactions within the ionic aggregates.[39–45]

From Figure 4, the aged membranes showed higher storage moduli and T_α values. These changes are likely resulting from the formation of the chemical species (e.g., anhydrides),

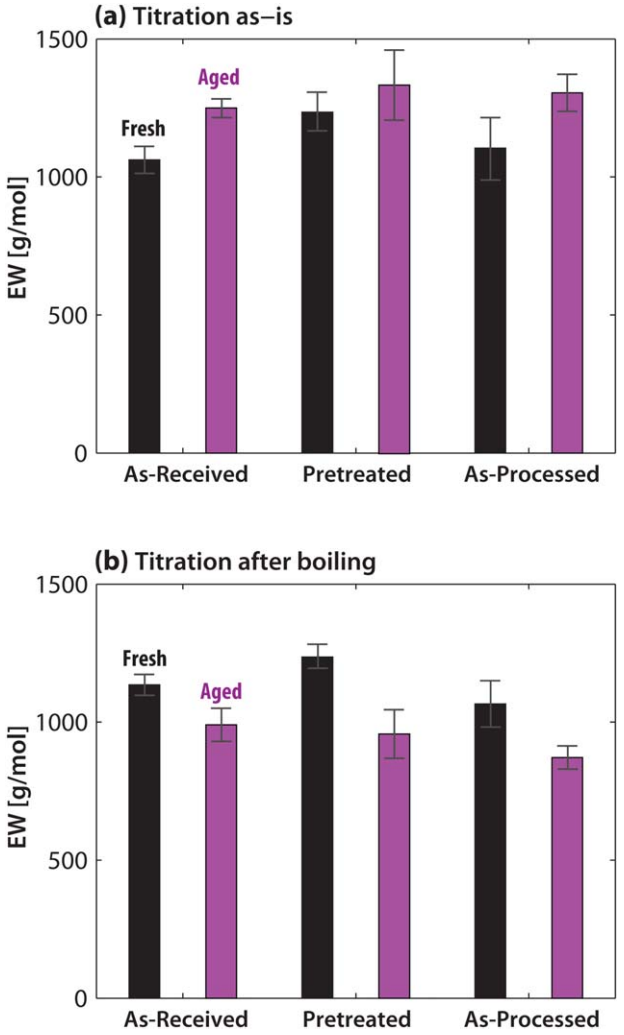

FIGURE 3 Equivalent weight of as-received (AsR), pretreated (PT), and as-processed (AsP) Nafion 212 membrane before and after hygrothermal aging. EW was measured by titrating the samples (a) as is (e.g., *as aged*), and (b) after boiling them in acid and water for 1 h. [Color figure can be viewed in the online issue, which is available at wileyonlinelibrary.com.]

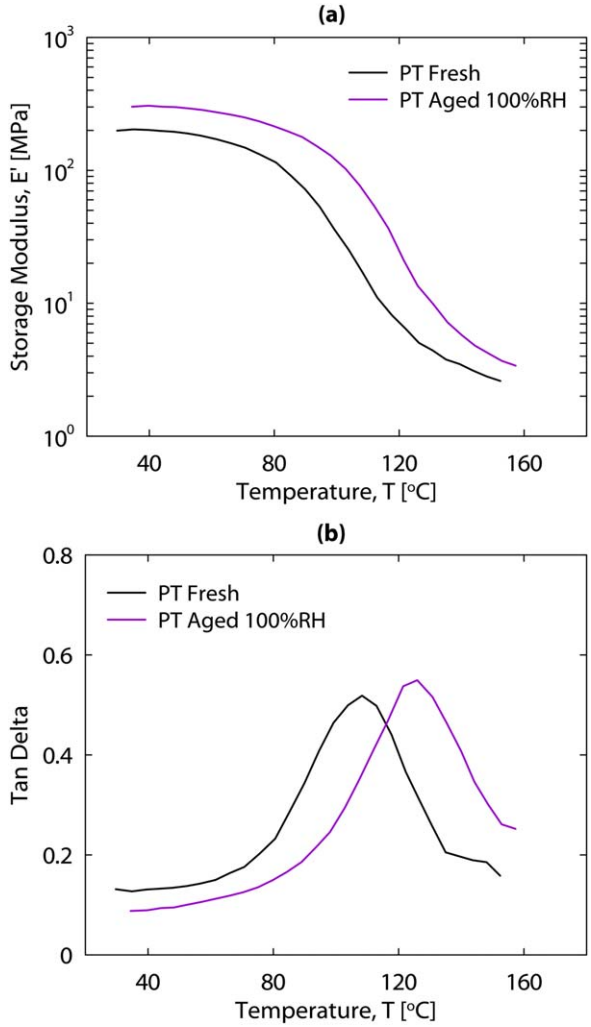

FIGURE 4 Dynamic mechanical responses of Nafion 212 PT membrane as a function of temperature for (a) storage modulus (b) tangent delta. [Color figure can be viewed in the online issue, which is available at wileyonlinelibrary.com.]

which may act as crosslinks between the polymer chains. These species delay the destabilization of the electrostatic interactions, and therefore increasing the transition temperature. Such results are consistent with the observed increase of EW.

To determine whether the mechanical property changes are due solely to the higher EW and not increased crystallinity, WAXS was done as summarized in Figure 5. From the figure, there is no discernable change in crystallinity with aging, which is consistent with the observations by Collette et al.[10] Such a finding can be contrasted with thermal annealing, where we previously observed an increase in the WAXS peak and therefore in relative degree of crystallinity [see Ref. 27 for details]. Thus, although both aging and annealing are known to increase mechanical properties by altering the thermal history of the membrane, it seems that aging-driven changes in mechanical properties appear to be due to crosslinking at sulfonic-acid sites, rather than a change in crystallinity.

Water Uptake

Figure 6 shows the normalized water uptake of fresh and aged Nafion membranes for two different pretreatments: PT and AsP. Comparison of the fresh sample data demonstrates very similar sorption isotherms for PT and AsP membranes, suggesting that hot pressing alone does not cause a significant change in water uptake. However, the influence of pretreatment is observed for the aged membranes, with the AsP membrane experiencing a larger impact of aging. Since the AsP samples were hot-pressed using PT samples, it seems that it was the hot-pressing process that caused this difference, which also is witnessed in the increased FTIR peak for AsP compared to PT samples. For PT membranes, hygrothermally aged samples are similar to the fresh samples, while the trend was quite different for AsP membranes, where the AsP membranes exhibited a significant reduction in water uptake at all humidities upon hygrothermal aging.

It should be noted that the impact of the EW change is implicitly considered since the uptake is normalized per sulfonic acid group (i.e., EW is related to the number of accessible SO_3 groups for a given quantity of polymer, whereas λ is nominally the number of water molecules associated with each of those SO_3 groups). Thus, the reduced uptake cannot be solely due to less available ionic groups), but due to an overall decrease in the membrane's water-uptake capacity driven by the changes in local environment and increased modulus altering the underlying chemical/mechanical energy balance.[27]

To understand the differences between the PT and AsP membranes better, water uptake in liquid water and close to saturated vapor (i.e., 98% RH) are compared in Figure 7. The water content, λ, is found to be higher in liquid water than

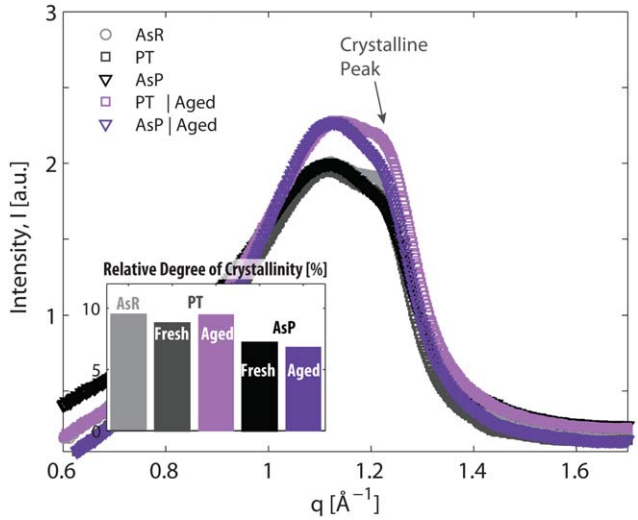

FIGURE 5 WAXS profiles of fresh and aged Nafion membranes showing the amorphous and crystalline peaks. Inset at the bottom shows the relative degree of crystallinity calculated from the crystalline and amorphous components of the WAXS peak. [Color figure can be viewed in the online issue, which is available at wileyonlinelibrary.com.]

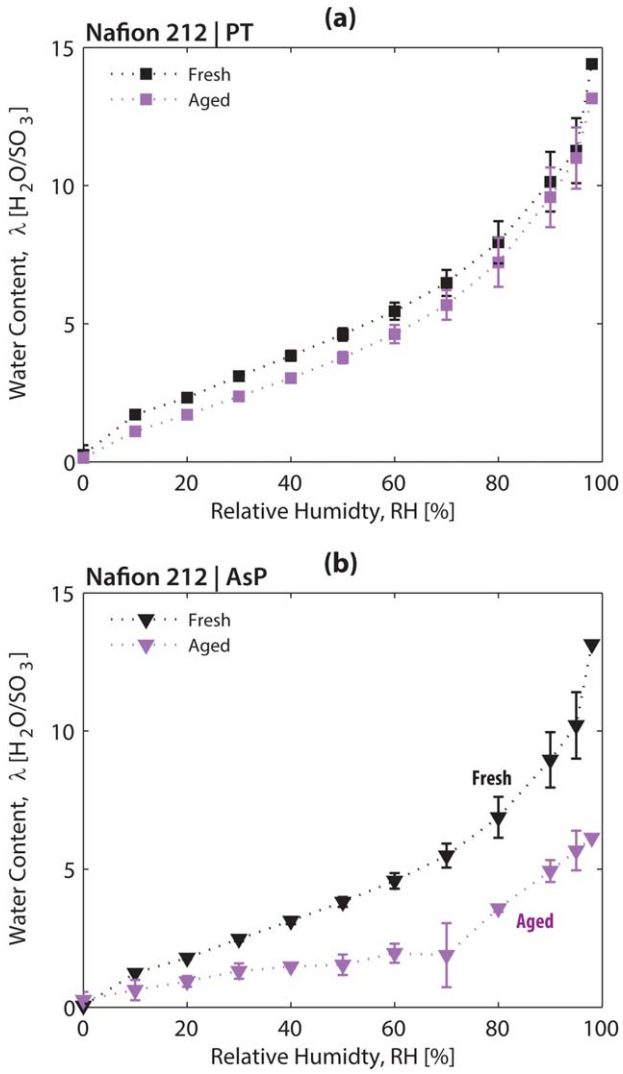

FIGURE 6 Water sorption isotherm of (a) pretreated and (b) as-processed Nafion 212 membrane measured through the weight change at 25 °C, before and after aging. Water content values are determined using the EWs corresponding to the treatment and aging conditions [shown in Fig. 3(a)]. [Color figure can be viewed in the online issue, which is available at wileyonlinelibrary.com.]

in saturated vapor, due to the commonly observed vapor/liquid transition (or so-called Schroeder's Paradox[46]).

As was the case with vapor, in liquid water, AsP membranes uptake less water than PT membranes, and aging results in a larger decrease in water content for AsP membranes, although there is some increased water uptake and partial recovery with temperature due to membrane softening and chain relaxation.[23,27,29]

Small-Angle X-Ray Scattering (SAXS)

To examine changes Figures 8 and 9 illustrate the SAXS profiles of hydrated membranes with different pretreatments as well as with different aging conditions. SAXS profiles exhibit two peaks typical of a PFSA ionomer: one at low-q (ca. 0.05 $Å^{-1}$), known as the intercrystalline peak or *matrix knee* corresponding the distance between the crystalline domains, and another peak at higher-q (ca. 0.14 $Å^{-1}$), termed the *ionomer peak* that is associated with the spacing of the hydrated hydrophilic domains.[10,27–29,40,47,48] Figure 8 clearly shows that pretreating an AsR membrane increases its water-domain size accompanied by a slight decrease in the intensity of the intercrystalline peak, in line with previous findings.[26,27] Also, this increase in domain size upon boiling is consistent with the increase in water content (Fig. 7) and indicate the expansion of nanodomains during the boiling process.[26,27] Compared with the AsR membranes, the ionomer peak of both PT and AsP membranes all shift to the left, indicating a larger d-spacing or hydrophilic domain spacing. Nevertheless, an interesting effect observed here is that hot-pressing of a PT membrane results in a

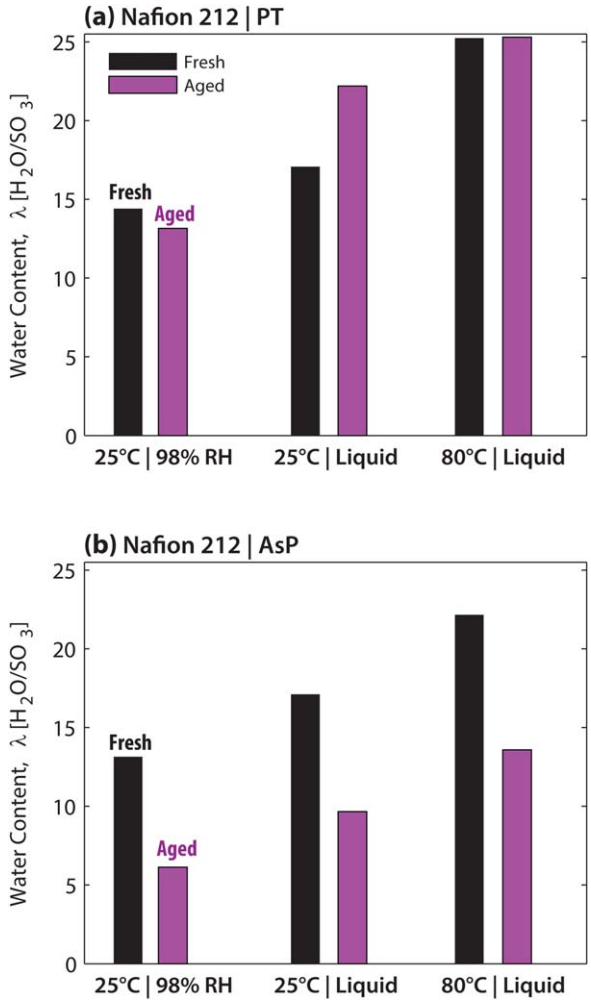

FIGURE 7 Water content of (a) pretreated and (b) as-processed membrane close to saturated vapor (98% RH) at 25 °C, and in liquid water at 25 and 80 °C measured before and after aging. To calculate water content at 80 °C, EW values measured after boiling the sample are used [shown in Fig. 3(b)], for consistency with thermal history. [Color figure can be viewed in the online issue, which is available at wileyonlinelibrary.com.]

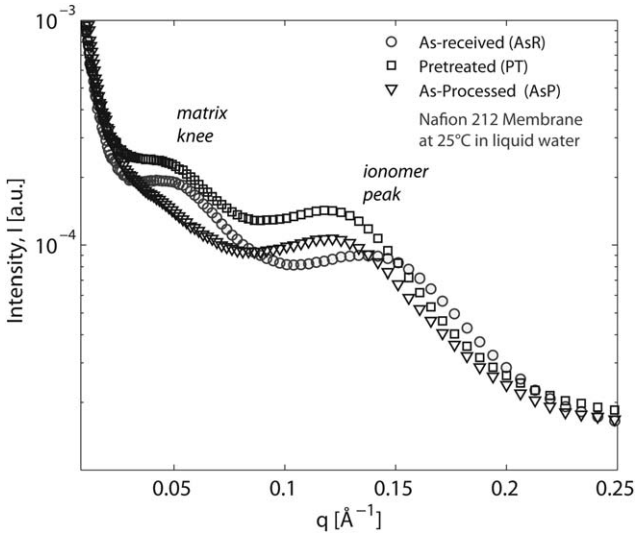

FIGURE 8 SAXS profiles of fresh Nafion ionomer undergone different pretreatments showing the characteristic scattering features of PFSA.

broader and less apparent intercrystalline peak even though the ionomer peak position remains almost the same.

Figure 9a,b compare the SAXS profiles of the liquid-equilibrated membrane before and after aging. The scattering profile of the PT membrane shows negligible change upon aging, similar to the case for the water-sorption isotherm [Fig. 6(a)]. The AsP membrane on the other hand exhibits a big rightward shift in ionomer peak after aging [Fig. 9(b)], indicating smaller water domains, again consistent with the decrease in water content [Fig. 7(b)]. Also, the crystalline peak changes in the same way the ionomer peak does, but to a lesser degree. In an effort to generate a structure-uptake dataset, SAXS experiments were also carried out *in situ* during heating the samples in liquid water and the resultant profiles are shown at selected temperatures (Fig. S1 in Supporting information).

From these data one can correlate the water-domain spacing, d_w, and intercrystalline spacing, d_c as shown in Figure 10. The results indicate a strong linear governing relationship between d_c and d_w, with all of the fresh and aged membranes falling on the same line, regardless of their pretreatment. Overall, pretreatment increases d_w, which pushes the crystalline domains further apart (larger d_c) to accommodate the larger water domains. Upon aging, the trend is reversed such that shrinking water domains yield decreased intercrystalline distance. It is worth nothing that the change in intercrystalline distance for aged membrane does not necessarily imply a change in crystallinity, which was observed to be insensitive to aging (Fig. 5).

Conductivity

The through-plane conductivity of fresh and aged membranes is shown in Figure 11. The conductivity of the PT membrane significantly decreased after aging, showing the same trend as seen with the water uptake: the higher the EW of the membrane, the lower the conductivity; this is consistent with less available sulfonic-acid groups that participate in conduction. Interestingly, the conductivity is lower even at the same water content. Taking into account the relationship between humidity and water content, λ, shown in Figure 6, one can plot the conductivity as a function of water content [Fig. 11(b)]. Thus, conductivity at a given λ decreases with increasing EW (e.g., aging), while the almost linear relationship between κ and λ is preserved for all samples. Hence, the slope representing the κ/λ can be described as a parameter related to the structure/functionality of the membrane changing with EW.

To investigate possible recovery and reversibility of the aging, the in-plane conductivity of PT membranes before and after aging and post-treatments were measured (Fig. 12). The in-plane conductivity showed the same trend as the

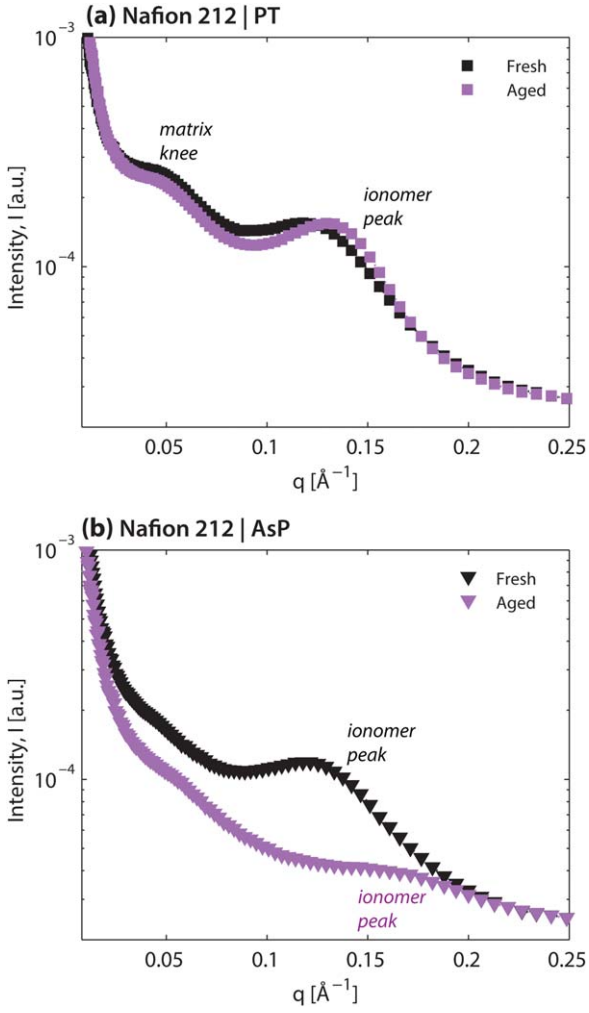

FIGURE 9 SAXS profiles of fresh and aged Nafion membrane for (a) pretreated and (b) as-processed samples showing the change in peak behavior upon hygrothermal aging. [Color figure can be viewed in the online issue, which is available at wileyonlinelibrary.com.]

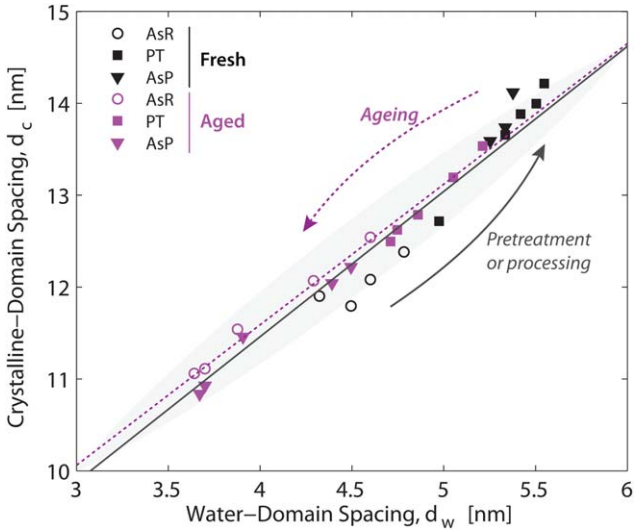

FIGURE 10 Correlation of intercrystalline domain spacing with water-domains spacing during heating in liquid water for fresh and aged Nafion membrane. d_c and d_w are determined from the peak positions of matrix knee and ionomer peak, respectively (see Fig. 8). A universal relationship is observed between the increased crystalline packing (reduced spacing) and reduced water-domain spacing. [Color figure can be viewed in the online issue, which is available at wileyonlinelibrary.com.]

through-plane conductivity, with the fresh membrane having the highest conductivity and the aged membrane the lowest. After immersing these membranes in water for 24 h, the conductivity of both membranes increased slightly. After boiling these membranes in water, the conductivity increased further, presumably because these membranes reached a quasi-equilibrium state after boiling,[23,27] although the subsequent values were still lower than that of the fresh ones, implying that the aging effect was not erased completely by this post-treatment. However, boiling the membranes in acid resulted in values that were essentially the same as the fresh ones; thus the aging is somewhat reversible, unlike chemical degradation.

DISCUSSION

The above systematic investigation allows one to probe and explore the changes due to aging on the underlying structure/function relationship of the PFSA membrane. The data are consistent with the reduction in available sulfonic-acid groups (i.e., increase in EW) due to hygrothermal aging, which results in the formation of a functional species (e.g., anhydrides) giving rise to the FTIR peak at 1440 cm^{-1}. These functional groups act as crosslinks between the polymer chains and thus increase the EW and can be associated with increasing mechanical properties of the membrane. Unlike thermal annealing, crystallinity does not change. The change in mechanical properties as well as chemical changes to the local environment, for example, the formation of sulfonic anhydride which is less hydrophilic than sulfonate,[3] results in lower water contents and a shift in the underlying chemical/mechanical energy balance that drives water uptake.[27] The SAXS data are consistent with this in that after aging, the ionomer peak shifts significantly to the right and broadens, implying a wider distribution of smaller and maybe even isolated water domains.

This change in domain distribution results in a more severe decrease in ionic conductivity than changes in EW and water uptake (e.g., after aging, the conductivity decreases by 50% whereas the increase in EW was at most 25%). This trend is consistent with the observations by Collette et al.[10] as well as by Clapham et al.,[9] who reported a conductivity loss of 80 versus 49% increase in EW.[9] Similarly, aging results in a more dramatic decrease in conductivity than water content. Such a finding can be explained by the different

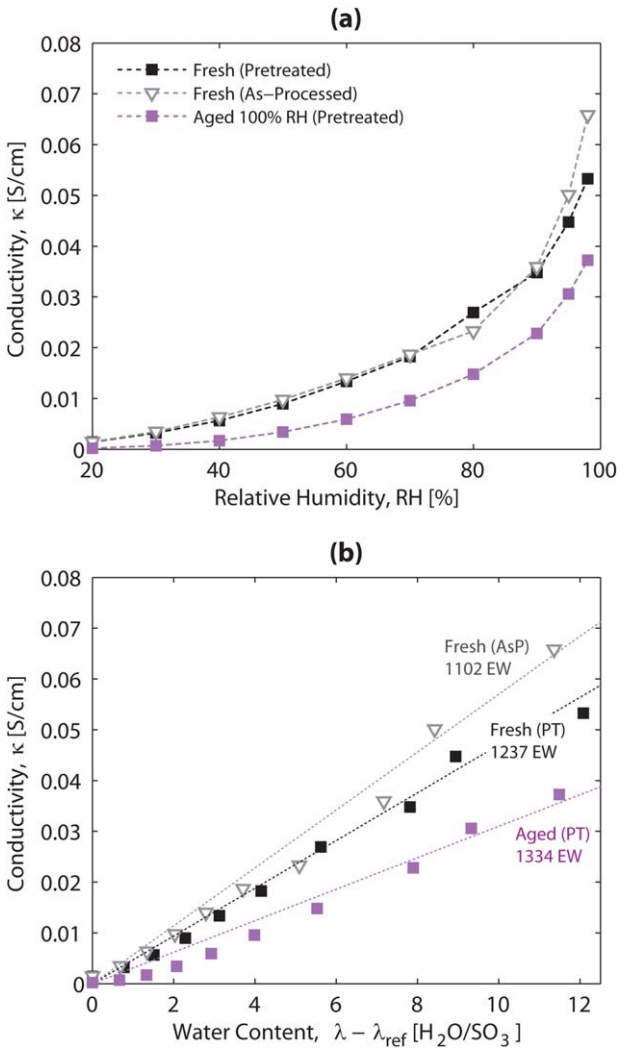

FIGURE 11 Through-plane conductivity of fresh and aged Nafion membranes as a function of (a) relative humidity and (b) change in water content at 30 °C. The change water content is calculated with respect to the value of λ at 20% RH, λ_{ref}, which is approximately 2 [see Refs. 27,29,49]. [Color figure can be viewed in the online issue, which is available at wileyonlinelibrary.com.]

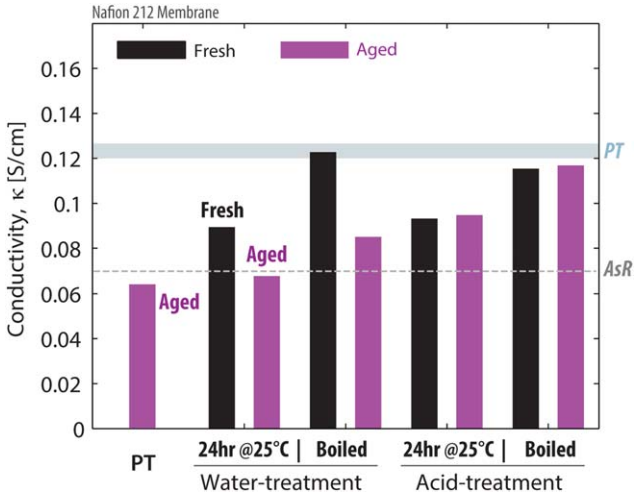

FIGURE 12 In-plane conductivity of fresh and aged pretreated Nafion membrane measured in water before and after various post-treatments. AsR (as-received) and PT (pretreated) lines represent the conductivity of fresh membrane pretreated for comparison. [Color figure can be viewed in the online issue, which is available at wileyonlinelibrary.com.]

nanostructure, especially the connectivity of the domains that along the number of sites, dominates the mobility.[9,10,48,50,51] Thus, it is not surprising to observe that aging influences the SAXS ionomer peak in a similar way it influences the conductivity. The fact that the most dramatic change in SAXS profiles is the dramatic broadening of the ionomer peak (i.e., distribution of domain sizes), more so than the location of the peak, strongly implies the critical role of aging-induced changes in connectivity on transport properties. The findings herein provide supporting evidence and help resolve the observations of Clapham et al., who reported a discrepancy between the IEC values and the integrated area of the SO_3^- band from the IR spectra.[9]

From the SAXS ionomer peak positions (see Supporting Information Fig. S1), water domain spacing, d_w, is determined in liquid water with respect to its value in dry state at room temperature. Figure 13 demonstrates that d_w changes with λ linearly such that all the d_w–λ data pairs for the fresh membranes reside on the same line, as shown previously,[27] and is consistent with changes in chemical (hydration) and mechanical (deformation) energy balance due to temperature and pretreatment. However, unexpectedly, Figure 13 demonstrates that this underlying relationship is altered upon aging, which consistently reduces the d-spacing but not necessarily λ (i.e., aging does not just move one down the same d–λ curve). After aging, AsP membranes exhibit the largest decrease in λ, whereas the AsR and PT membranes have higher λ. Moreover, even though the aged samples' domain spacing increase during heating in liquid water, which is a post-treatment process, they do not fully recover their initial values despite an increase in water content, revealing important morphological changes where the aging-induced crosslinks prevent expansion of water domains and perhaps reducing their connectivity as well. Thus, this structure–swelling correlation helps understand better the true impact of aging and recovery.

The impact of thermal history seems to have a profound impact on the result of aging. For all of the characterization, the PT membrane appears to be less sensitive to aging compared to the AsP membrane in terms of transport, uptake, and structural properties. This is consistent with the increased amount of anhydrides for AsP compared to PT membranes, which not only exhibited decreased water content, but also a different water-uptake profile (see Fig. 7). As mentioned, AsP membranes were hot pressed and then aged; however, just the hot-pressing did not seem to result in a change in the water-domain spacing (Fig. 8) and water content (Fig. 7), yet it appears to influence the distribution of the crystalline domains and overall crystallinity (see Fig. 5). The influence of pretreatment on the SAXS profiles manifests itself even stronger after aging, where the AsP membrane exhibits a big rightward shift in ionomer peak after aging [Fig. 9(b)], indicating smaller water domains, again consistent with the decrease in water content [Fig. 7(b)]. The reason for this increased impact on the AsP membranes could be due to the fact that the hot-pressing resulted in an increased propensity for initiation of crosslink formation perhaps due to the introduction or exacerbation of potential reactive sites or presence of foreign cations. For example, Collette et al.[10] reported an increase in the anhydride content and accelerated aging with

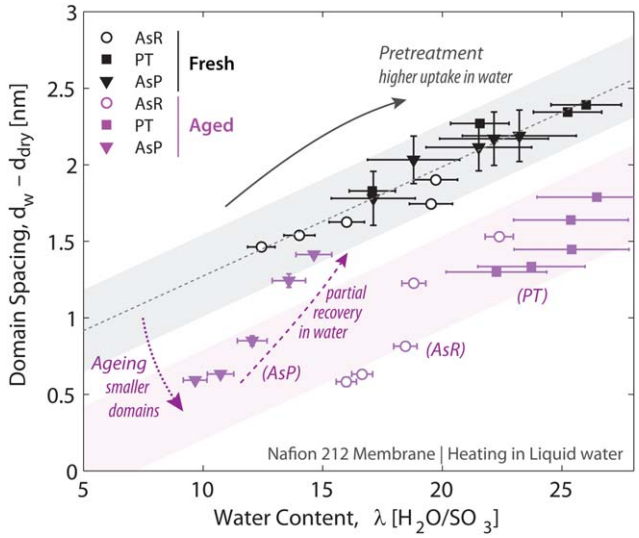

FIGURE 13 Change in water domain spacing with water content during heating in liquid water (from 25 to 90 °C) for fresh and aged Nafion membrane obtained from the SAXS data (change in domain spacing is determined from the ionomer peak position of the hydrated samples with respect to their value in ambient conditions). Plot shows that pretreatment increases the domain spacing and water content, that is, "nano-swelling", which is then reduced upon hygrothermal aging. The bands for the fresh and aged samples are guide for-the-eye. [Color figure can be viewed in the online issue, which is available at wileyonlinelibrary.com.]

a cationic pollutant. In addition, Clapham et al.[9] found that the intensity of the FTIR band at 1440 cm^{-1} after aging increased with membrane thickness, which can also be interpreted as the existence of other phenomena than anhydride formation. The fact that pretreated membrane exhibits less change in nanostructure and water uptake with aging compared with an as-received membrane supports the potential role of contaminants, which is likely to be eliminated during the pretreatment process. In addition, during operation, such contamination may also exist depending on the application. It may also be that AsP membranes resulted in different surface or bulk structures which enhance reactions forming other functional species, something that is under current investigation.

The weak effect of aging for the PT membranes can be explained by the fact that these membranes have larger domains and therefore longer distance between the SO_3^- groups, which makes the condensation reaction less favorable. Such a concept aligns with reports that for as-received membranes, aging at higher humidities is less effective in forming anhydrides both because of the above mentioned morphological difference as well as the fact that anhydride hydrolysis might take place and dominate in the presence of water.[10] In fact, we have seen that aging at 75% RH results in an even higher intensity of the 1440 cm^{-1} peak with the expected concomitant change in properties (see Supporting Information Fig. S2), an issue that deserves further study seeing as PEFCs are typically operated at lower humidities for a good portion of the cell planform. However, the fact that aging at the same RH, and therefore for the same water content, results in a large decrease in the sorption capacity of the AsP (i.e., hot-pressed) membranes implies that the pretreatment plays a key role in facilitating the condensation reactions.

Recovery of the various properties of the aged membranes, especially conductivity, occurred after acid treatment (Fig. 12). Acid treatments and higher water contents promote the hydrolysis of the anhydride groups. The removal of aging-induced functional species upon acid treatment was corroborated by the FTIR data which shows the peak disappears after boiling in acid, but not after boiling in water (see Supporting Information Fig. S3), consistent with the conductivity observations. From the data, it appears that some of the unavailable SO_3^- groups in aged ionomer became accessible after boiling, especially in acid, which could also be attributed to removal of cationic contaminants. The morphology, especially the ionomer peak, of aged membranes is also recovered after boiling (see Supporting Information Fig. S3). In addition, the mechanical properties of aged membranes returned to their initial values after boiling (see Supporting Information Fig. S4). Heating of the aged membranes closer to the boiling temperature resulted in partial recovery in the SAXS profiles as well (Supporting Information Fig. S1), consistent with less crosslinks. Hence, the fact that conductivity, mechanical properties, EW, and nanostructure all change in a consistent manner both during aging and after recovery due to post-treatments provide a compelling evidence for the key roles they have in controlling the structure/property relationship of PFSA membranes. During PEFC operation the membrane is exposed to high temperatures and liquid water, which is likely to change its effective EW and transport properties.

CONCLUSIONS

In this paper, the impact of hygrothermal aging on the nanostructure and properties of Nafion membranes was explored, with particular focus on changes in the structure–property correlation during aging. It was shown that hygrothermal aging leads to formation of a functional group at a FTIR absorbance of 1440 cm^{-1}, which has been assigned to anhydride species. This resulted in an increase in equivalent weight with a subsequent decrease in water uptake and conductivity. Exploration of the nanoscale morphology demonstrated that both the water and intercrystalline domain spacing varied with the aging process, although not on the same intrinsic λ–d_w line observed for fresh membranes, thereby indicating morphological changes beyond the loss of sulfonic acid accessibility. Mechanical properties also demonstrated increased moduli and transition temperatures with aging. Of note is that pretreatment had a substantial effect on the impact of aging, wherein the pretreated membrane did not show significant differences in properties with aging as compared to as-received ones. However, if the pretreated membranes were processed, that is, hot-pressed, prior to aging, the impact of aging was exacerbated as the hot-pressing process seemingly converted the pretreated membrane to its initial, as-received form. The resultant impacts of aging were shown to be relatively reversible with various levels of recovery being obtained through heating in water and acid. This study demonstrates the importance of hygrothermal aging and membrane pretreatment on underlying membrane properties, and has impacts on various technologies including fuel cells, redox flow batteries, and membrane humidifiers.

ACKNOWLEDGMENTS

The authors would like to thank Kyle T. Clark for his help with using some of the diagnostics equipment. AK and AZW thank C.G. Gittleman of General Motors for insightful discussions. SAXS/WAXS experiments were performed in the beamline 7.3.3 at Advanced Light Source (ALS), Lawrence Berkeley National Laboratory, which is a national user facility funded by the Department of Energy, Office of Basic Energy Sciences, under contract number DE-AC02-05CH11231. We thank Chenhui Zhu and Dr. Eric Schiable for their assistance during facilitating the use of equipment at ALS. Shouwen Shi greatly thanks China Scholarship Council (CSC) for financial support during his visit to Lawrence Berkeley National Laboratory. This work was funded by the Assistant Secretary for Energy Efficiency and Renewable Energy, Fuel Cell Technologies Office, of the U. S. Department of Energy under contract

number DE-AC02-05CH11231 (LBNL) and Program Development Managers Donna Ho and Nancy Garland.

REFERENCES AND NOTES

1 A. Kusoglu, M. Calabrese, A. Z. Weber. *Ecs Electrochem. Lett.* **2014**, *3*, F33–F36.

2 Gittleman, C. S.; Coms, F. D.; Lai, Y.-H. In Polymer Electrolyte Fuel Cell Degradation; Matthew, M.; Emin Caglan, K.; Veziroglu, T. N., Eds.; Academic Press: Boston, **2012**, p 15–88.

3 F. M. Collette, C. Lorentz, G. Gebel, F. Thominette, *J. Membr. Sci.* **2009**, *330*, 21–29.

4 Lim, L. Ghassemzadeh, F. Van Hove, M. Lauritzen, J. Kolodziej, G. G. Wang, S. Holdcroft, E. Kjeang, *J. Power Sources* **2014**, *257*, 102–110.

5 Kusoglu, M. H. Santare, A. M. Karlsson, S. Cleghorn, W. B. Johnson, *J. Electrochem. Soc.* **2010**, *157*, B705–B713.

6 M. P. Rodgers, L. J. Bonville, R. Mukundan, R. L. Borup, R. Ahluwalia, P. Beattie, R. P. Brooker, N. Mohajeri, H. R. Kunz, D. K. Slattery, J. M. Fenton, *ECS Trans.* **2013**, *58*, 129–148.

7 M. P. Rodgers, L. J. Bonville, H. R. Kunz, D. K. Slattery, J. M. Fenton, *Chem. Rev.* **2012**, *112*, 6075–6103.

8 F. M. Collette, F. Thominette, S. Escribano, A. Ravachol, A. Morin, G. Gebel, *J. Power Sources* **2012**, *202*, 126–133.

9 S. M. Clapham, F. D. Coms, T. J. Fuller, L. Zou, *ECS Trans.* **2013**, *50*, 1011–1020.

10 F. M. Collette, F. Thominette, H. Mendil-Jakani, G. Gebel, *J. Membr. Sci.* **2013**, *435*, 242–252.

11 S. Naudy, F. Collette, F. Thominette, G. Gebel, E. Espuche, *J. Membr. Sci.* **2014**, *451*, 293–304.

12 S. Shi, G. Chen, Z. Wang, X. Chen, *J. Power Sources* **2013**, *238*, 318–323.

13 M. Casciola, G. Alberti, M. Sganappa, R. Narducci, *Desalination* **2006**, *200*, 639–641.

14 J. T. Uan-Zo-li, Master Thesis, Virginia Polytechnic Institute and State University, Blacksburg, VA, **2001**.

15 T. F. Fuller, *Polym. Degrad. Stab.* **2009**, *94*, 1436–1447.

16 W. Yoon, X. Y. Huang, *J. Electrochem. Soc.* **2010**, *157*, B599–B606.

17 T. Xie, K. A. Page, S. A. Eastman, *Adv. Funct. Mater.* **2011**, *21*, 2057–2066.

18 G. Alberti, R. Narducci, *Fuel Cells* **2009**, *9*, 410–420.

19 G. M. Divoux, K. A. Finlay, J. K. Park, J. M. Song, B. Yan, M. Zhang, D. A. Dillard, R. B. Moore, *ECS Trans.* **2011**, *41*, 87–100.

20 J. T. Hinatsu, M. Mizuhata, H. Takenaka, *J. Electrochem. Soc.* **1994**, *141*, 1493–1498.

21 L. Maldonado, J. C. Perrin, J. Dillet, O. Lottin, *J. Membr. Sci.* **2012**, *389*, 43–56.

22 E. Evans, R. D. Noble, S. Nazeri-Thompson, B. Nazeri, C. A. Koval, *J. Membr. Sci.* **2006**, *279*, 521–528.

23 L. M. Onishi, J. M. Prausnitz, J. Newman, *J. Phys. Chem. B* **2007**, *111*, 10166–10173.

24 J. E. Hensley, J. D. Way, S. F. Dec, K. D. Abney, *J. Membr. Sci.* **2007**, *298*, 190–201.

25 G. Gebel, P. Aldebert, M. Pineri, *Macromolecules* **1987**, *20*, 1425–1428.

26 J. A. Elliott, S. Hanna, J. N. Newton, A. M. S. Elliott, G. E. Cooley, *Polym. Eng. Sci.* **2006**, *46*, 228–234.

27 A. Kusoglu, S. Savagatrup, K. T. Clark, A. Z. Weber, *Macromolecules* **2012**, *45*, 7467–7476.

28 Y. Liu, J. L. Horan, G. J. Schlichting, B. R. Caire, M. W. Liberatore, S. J. Hamrock, G. M. Haugen, M. A. Yandrasits, S. Seifert, A. M. Herring, *Macromolecules* **2012**, *45*, 7495–7503.

29 A. Kusoglu, A. Z. Weber, In Polymers for Energy Storage and Delivery: Polyelectrolytes for Batteries and Fuel Cells; American Chemical Society: Washington, **2012**, pp 175–199.

30 T. A. Zawodzinski, C. Derouin, S. Radzinski, R. J. Sherman, V. T. Smith, T. E. Springer, S. J. Gottesfeld, *Electrochem. Soc.* **1993**, *140*, 1041–1047.

31 T. Y. Chen, J. Leddy, *Langmuir* **2000**, *16*, 2866–2871.

32 S. Slade, S. A. Campbell, T. R. Ralph, F. C. Walsh, *J. Electrochem. Soc.* **2002**, *149*, A1556–A1564.

33 L. A. Zook, J. Leddy, *Anal. Chem.* **1996**, *68*, 3793–3796.

34 T. E. Springer, T. A. Zawodzinski, S. Gottesfeld, *J. Electrochem. Soc.* **1991**, *138*, 2334–2342.

35 J. D. Menczel, R. B. Prime, Thermal Analysis of Polymers, Fundamentals and Applications; Wiley, New York, **2009**.

36 K. R. Cooper, *J. Electrochem. Soc.* **2010**, *157*, B1731–B1739.

37 R. J. Roe, Methods of X-ray and Neutron Scattering in Polymer Science; Oxford University Press, Oxford, **2000**.

38 Moukheiber, G. De Moor, L. Flandin, C. Bas, *J. Membr. Sci.* **2012**, *389*, 294–304.

39 T. Kyu, M. Hashiyama, A. Eisenberg, *Can. J. Chem.* **1983**, *61*, 680–687.

40 K. A. Page, F. A. Landis, A. K. Phillips, R. B. Moore, *Macromolecules* **2006**, *39*, 3939–3946.

41 S. J. Osborn, M. K. Hassan, G. M. Divoux, D. W. Rhoades, K. A. Mauritz, R. B. Moore, *Macromolecules* **2007**, *40*, 3886–3890.

42 B. Matos, E. Santiago, J. Rey, F. Fonseca, *Phys. Rev. E* **2014**, *89*, 052601.

43 S. C. Yeo, A. Eisenberg, *J. Appl. Polym. Sci.* **1977**, *21*, 875–898.

44 K. A. Page, K. M. Cable, R. B. Moore, *Macromolecules* **2005**, *38*, 6472–6484.

45 K. A. Page, J. K. Park, R. B. Moore, V. G. Sakai, *Macromolecules* **2009**, *42*, 2729–2736.

46 P. Z. Schroeder, *Phys. Chem.* **1903**, *45*, 75.

47 Gebel, *Polymer* **2000**, *41*, 5829–5838.

48 A. Kusoglu, A. Hexemer, R. C. Jiang, C. S. Gittleman, A. Z. Weber, *J. Membr. Sci.* **2012**, *421*, 283–291.

49 Z. Weber, J. Newman, *J. Electrochem. Soc.* **2004**, *151*, A311–A325.

50 A. Wang, V. Krishnan, D. Wu, R. Bledsoe, S. J. Paddison, G. Duscher, *J. Mater. Chem. A* **2013**, *1*, 938–944.

51 P. A. García-Salaberri, G. Hwang, M. Vera, A. Z. Weber, J. T. Gostick, *Int. J. Heat Mass Transf.* **2015**, *86*, 319–333.